Relation between random walks and quantum walks

Stefan Boettcher,[1] Stefan Falkner,[1] and Renato Portugal[2]
[1]*Department of Physics, Emory University, Atlanta, Georgia 30322, USA*
[2]*Laboratório Nacional de Computação Científica, Petrópolis, Rio de Janeiro 25651-075, Brazil*
(Received 31 October 2014; published 29 May 2015)

Based on studies of four specific networks, we conjecture a general relation between the walk dimensions d_w of discrete-time random walks and quantum walks with the (self-inverse) Grover coin. In each case, we find that d_w of the quantum walk takes on exactly half the value found for the classical random walk on the same geometry. Since walks on homogeneous lattices satisfy this relation trivially, our results for heterogeneous networks suggest that such a relation holds irrespective of whether translational invariance is maintained or not. To develop our results, we extend the renormalization-group analysis (RG) of the stochastic master equation to one with a unitary propagator. As in the classical case, the solution $\rho(x,t)$ in space and time of this quantum-walk equation exhibits a scaling collapse for a variable x^{d_w}/t in the weak limit, which defines d_w and illuminates fundamental aspects of the walk dynamics, e.g., its mean-square displacement. We confirm the collapse for $\rho(x,t)$ in each case with extensive numerical simulation. The exact values for d_w themselves demonstrate that RG is a powerful complementary approach to study the asymptotics of quantum walks that weak-limit theorems have not been able to access, such as for systems lacking translational symmetries beyond simple trees.

DOI: 10.1103/PhysRevA.91.052330 PACS number(s): 03.67.Ac, 05.10.Cc, 05.40.Fb

I. INTRODUCTION

Like random walks, quantum walks are rapidly gaining a central role in describing a considerable range of phenomena, from experiments in quantum transport [1–4] to universal models of quantum computing [5,6]. Quantum walks are the "engine" that drives quantum search algorithms [7], with the prospect of a quadratic speedup over classical search algorithms. However, despite considerable efforts, our understanding of quantum walks still lags behind that of random walks [8–11], as quantum walks exhibit a much broader spectrum of behaviors awaiting categorization and context, even for simple lattices [12–21].

For random walks, the probability density $\rho(\vec{x},t)$ to detect a walk at time t at site $\vec{x}$, a distance $x = |\vec{x}|$ from its origin, obeys the scaling collapse [9],

$$\rho(\vec{x},t) \sim t^{-\frac{d_f}{d_w}} f\left(x/t^{\frac{1}{d_w}}\right), \tag{1}$$

with the scaling variable $x/t^{1/d_w}$, where d_f is the (possibly fractal) dimension of the network. On a translationally invariant lattice in any spatial dimension $d(=d_f)$, it is easy to show that the walk is always purely "diffusive", $d_w = 2$, with a Gaussian scaling function f, which is the content of many classic textbooks on random walks and diffusion [10,22]. The scaling in Eq. (1) still holds when translational invariance is broken in certain ways or the network is fractal (i.e., d_f is noninteger). However, anomalous diffusion with $d_w \neq 2$ may arise in many transport processes [9,23,24].

For quantum walks, the only known value for a finite walk dimension is that for ordinary lattices [25], where Eq. (1) generically holds with $d_w = 1$, indicating a "ballistic" spreading of the quantum walk from its origin. This value has been obtained for various versions of one- and higher-dimensional quantum walks, for instance, with so-called weak-limit theorems [17,20,25–27]. The renormalization-group (RG) method we have introduced recently [28] provides an alternative approach, expanding the analytic tools to understand quantum walks, since it works for networks that lack translational symmetries. While still short of the mathematical rigor of existing limit theorems, RG provides principally exact results in terms of the asymptotic scaling variable $x/t^{1/d_w}$ (or pseudovelocity [29]) whose existence allows us to collapse all data for the probability density $\rho(\vec{x},t)$, aside from oscillatory contributions ("weak limit"), as in Eq. (1).

Here we propose a relation bridging random and quantum walks that elucidates their scaling properties at long times and distances on arbitrary networks, which is intimately linked to the dynamics of their spread as well as their algorithmic performance [30,31]. We find that the walk dimension d_w for a discrete-time quantum walk with a Grover coin is half of that for the corresponding random walk,

$$d_w^{QW} = \tfrac{1}{2}\, d_w^{RW}. \tag{2}$$

Abstracting from four specific examples used in this paper, this relation might be rather general, and we show that it holds even if the walks are anomalous and the geometry lacks translational symmetry. A similar relation has been obtained for the return probability of a continuous-time quantum walk [32], where it is traced to the generic long-time dominance of the ground-state eigenvalue and the fact that ρ is based on the modulo square of the site amplitude, instead of linearly in the random-walk case. However, such a simple connection is not obvious here, as Eq. (2) is strongly coin dependent.

This ability to explore a given geometry that much faster than diffusion is essential for the effectiveness of quantum search algorithms [30,31]. While this value satisfies Eq. (2), it does little to justify it. [None of the existing theories, for instance, can distinguish Eq. (2) from, say, $d_w^{QW} = d_w^{RW} - 1$.] The simplicity and robustness of the value of d_w is surprising, even on a simple line, $d = 1$. We can picture $\rho(\vec{x},t)$ as resulting from the superposition of all paths that lead from the origin $\vec{x}_0 = 0$ to site $\vec{x}$ in t steps, weighted by the probability of each path. Classically, each path merely receives a factor $\frac{1}{2}$ for the probability to branch left or right at every step (in the simplest

case). Then, all paths have the *same* weight 2^{-t}, and $\rho(\vec{x},t)$ becomes distinguished only by the *number* of paths that can reach $\vec{x}$, with its variance after t steps, $\langle \vec{x}^2 \rangle \sim t$, providing $d_w = 2$. For the widely used description of a discrete-time quantum walk [13], $\rho(\vec{x},t)$ becomes the modulo squared of the weighted sum over the very same paths. At any branch, each path receives a *different* complex factor to its weight. It is then the subtle superposition of these complex weights and their interference in the square modulus that determine the spread of $\rho(\vec{x},t)$. Although quantum walks may possess extra internal degrees of freedom, asymptotically, they invariably result in $d_w = 1$.

The distinct manner in which random walks and quantum walks attain their respective probability densities $\rho(\vec{x},t)$ suggests that a relation between their walk dimensions, d_w^{RW} and d_w^{QW}, should be purely accidental. Any relation would be limited to a few geometries with special constraints on quantum interference effects, such as those imposed by translational invariance. Instead, based on a number of diverse *fractal* networks for which we have calculated nontrivial values of d_w for a widely used description of quantum walks, we find the succinct relation in Eq. (2), without exception, satisfied. This suggests that the common geometry leaves a deeper imprint on the long-time behavior of both random and quantum walks than might have been expected from their rather distinct dynamics. Such insight could make quantum-walk-based algorithms more predictable for networks [33].

This paper is organized as follows: In the next section, we introduce the formulation of the discrete-time quantum walk that we will use in the RG analysis. In Sec. III, we discuss the RG procedure using the example of the simplest of our networks, and we use it to discuss the results for all networks, with details of the calculations for most of those networks provided in the Appendix. In Sec. IV we conclude, discussing the implication of our results for universality, and give an outlook on future studies.

II. DISCRETE-TIME QUANTUM WALKS

The dynamics for a discrete-time walk with a coin, classical or quantum, is determined by the master equation,

$$|\Psi_{t+1}\rangle = \mathcal{U}|\Psi_t\rangle. \tag{3}$$

In the site basis $|\vec{x}\rangle$ of any network, we can describe the state of the system in terms of the site amplitudes $\psi_{\vec{x},t} = \langle \vec{x}|\Psi_t\rangle$. For a classical random walk, the probability density in Eq. (1) is simply given by the site amplitude itself, $\rho(\vec{x},t) = \psi_{\vec{x},t}$, while for the quantum walk it is $\rho(\vec{x},t) = |\psi_{\vec{x},t}|^2$. Accordingly, the propagator $\mathcal{U}$ is a stochastic Bernoulli coin for a random walk, while it must be *unitary* for a quantum walk, usually composed as

$$\mathcal{U} = \mathcal{S}(\mathbb{I} \otimes \mathcal{C}), \tag{4}$$

with coin $\mathcal{C}$ and shift $\mathcal{S}$. Unitarity, $\mathcal{U}^\dagger\mathcal{U} = \mathbb{I}$, demands [34,35] that the coin be a unitary matrix of rank $r > 1$, such that the site amplitudes $\psi_{\vec{x},t}$ become complex r-dimensional vectors in "coin" space. For simplicity, this quantum walk is commonly studied on networks of regular degree r for all $\vec{x}$, so that the same coin can be applied at every site. Every step consists of a "coin flip," the multiplication of $\psi_{\vec{x},t}$ with $\mathcal{C}$, followed by the shift $\mathcal{S}$ that transfers each component of $\mathcal{C} \cdot \psi_{\vec{x},t}$ to exactly one of the r neighbors of $\vec{x}$.

TABLE I. Fractal and walk dimensions for the networks considered here. The classical values for d_f and d_w^{RW} are known for DSG [9] and HN3 [38] and are derived here for MK. The values for d_w^{QW} are determined with the RG. Each case satisfies Eq. (2). We also provide the values for translationally invariant hypercubic lattices for reference.

Network	d_f	d_w^{RW}	d_w^{QW}
Lattice	d	2	1
MK3	$\log_4(7)$	$\log_4(21) \approx 2.196$	1.098079...
MK4	$\log_4(13)$	$\log_4\left(\frac{247}{7}\right) \approx 2.571$	1.285253...
HN3	2	$\log_2(24 - 8\sqrt{5}) \approx 2.612$	1.305758...
DSG	$\log_2(3)$	$\log_2(5) \approx 2.322$	1.160964...

To test Eq. (2) for nontrivial values of d_w, we study the quantum walk on four fractal networks of degrees $r = 3$ and 4, with the widely used Grover coin [7,21], i.e., the $r \times r$ matrix

$$\mathcal{C}_G^{(r)} = \frac{2}{r}\begin{pmatrix} 1-\frac{r}{2} & 1 & \cdots & 1 \\ 1 & \ddots & & \vdots \\ \vdots & & \ddots & 1 \\ 1 & \cdots & 1 & 1-\frac{r}{2} \end{pmatrix}. \tag{5}$$

Namely, we study two Migdal-Kadanoff networks [36,37] (MK3 and MK4), the dual Sierpinski gasket [9,11] (DSG), and the Hanoi network [38] (HN3). These networks lack translational invariance but exhibit self-similarity instead. DSG more closely resembles a $2d$ lattice, MK networks have a hierarchical structure, and HN3 is a hyperbolic [39] small-world network. For each network, the anomalous classical result for d_w of the random walk and its fractal dimension d_f are easily obtained via the RG method, which is discussed in many textbooks on statistical physics [11,37] and on transport properties [24]. (We have provided a simple primer in the context of quantum walks in [40].) We describe the application of RG below for MK3; the RG for MK4, DSG, and HN3 is discussed in the Appendix. By extending RG to quantum walks [28], we obtain the first exact scaling exponents for quantum walks on heterogeneous structures. All results are summarized in Table I.

III. QUANTUM-WALK RENORMALIZATION FOR MK3

The fractal dimension [9,11] is defined via the scaling $N \sim L^{d_f}$, where N stands for the number of sites that are at most L hops away from a given site. For MK3, as shown in Fig. 1, the number of edges (and hence sites) changes sevenfold between iterations, while distances between two sites changes fourfold, implying $d_f = \log_4(7)$.

To calculate the walk dimension with RG, we first apply the Laplace transform [10,11,24],

$$|\tilde{\Psi}(z)\rangle = \sum_{t=0}^{\infty} z^t |\Psi_t\rangle, \tag{6}$$

to Eq. (3), providing algebraic equations with generalized hopping operators that now depend on z. For instance, after

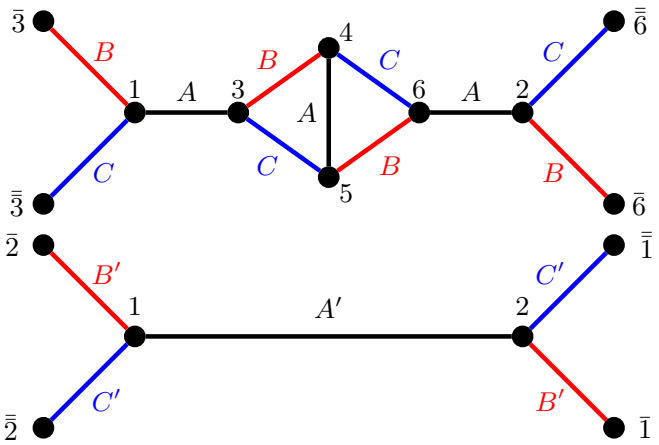

FIG. 1. (Color online) Iterative scheme for the decimation of the Migdal-Kadanoff network MK3. Interior sites 3, . . . ,6 in the graphlet (top) are algebraically eliminated [see Eq. (7)] and replaced by a single edge (bottom) with an effective ("renormalized") hopping operator A' by which the terminal site amplitudes 1,2 on either end of the edge shift their components between each other. (Edges from sites 1,2 to sites in equivalent neighboring structures are indicated by overbars.) While renormalization is shown only for an edge of type A, types B and C are obtained via cyclic permutation $A \to B \to C \to A$. Constructing MK3 for simulations proceeds by replacing every edge (bottom) by the corresponding graphlet (top) recursively for k iterations, as discussed in the Appendix.

any number of iterations, MK3 entirely consists of graphlets, as depicted in the top panel of Fig. 1. For sites 3, . . . ,6, it represents the *linear* system of equations [41]

$$\begin{pmatrix}\tilde{\psi}_3\\ \tilde{\psi}_4\\ \tilde{\psi}_5\\ \tilde{\psi}_6\end{pmatrix} = \begin{bmatrix} A & 0 & M & B & C & 0\\ 0 & 0 & B & M & A & C\\ 0 & 0 & C & A & M & B\\ 0 & A & 0 & C & B & M\end{bmatrix} \begin{pmatrix}\tilde{\psi}_1\\ \tilde{\psi}_2\\ \tilde{\psi}_3\\ \tilde{\psi}_4\\ \tilde{\psi}_5\\ \tilde{\psi}_6\end{pmatrix}, \quad (7)$$

with hopping operators A, B, C, and M, where M allows for self-interaction at each site. (In the original graph $M = 0$.) Taking advantage of self-similarity, we express one iteration of the network in terms of the next smaller one but with "renormalized" values for the hopping operators. To that end, we solve for $\tilde{\psi}_3, \ldots, \tilde{\psi}_6$ in terms of $\tilde{\psi}_1$ and $\tilde{\psi}_2$ and insert the result into the equations for the remaining site amplitudes, such that

$$\begin{aligned}\tilde{\psi}_{1,2} &= M\tilde{\psi}_{1,2} + A\tilde{\psi}_{3,6} + B\tilde{\psi}_{\bar{3},\bar{6}} + C\tilde{\psi}_{\bar{\bar{3}},\bar{\bar{6}}}\\ &= M'\tilde{\psi}_{1,2} + A'\tilde{\psi}_{2,1} + B'\tilde{\psi}_{\bar{2},\bar{1}} + C'\tilde{\psi}_{\bar{\bar{2}},\bar{\bar{1}}}, \end{aligned} \quad (8)$$

where primes indicate the renormalized hopping operators as depicted in the bottom panel of Fig. 1. Repetition then relates the $k+1$ (primed) iterate to the kth (unprimed) iterate, yielding the RG flow [24,37]

$$(A_{k+1}, B_{k+1}, C_{k+1}, M_{k+1}) = \mathcal{RG}(A_k, B_k, C_k, M_k), \quad (9)$$

which characterizes the effective dynamics between domains of sites of width L_k and L_{k+1} by renormalized hopping operators.

In the case of the unbiased random walk, all the hopping operators become simple scalars, $A = B = C = a$, and setting $M = 1 - b$, Eq. (9) provides

$$\begin{aligned} a_{k+1} &= \frac{2a_k^4}{b_k^3 - 4a_k^2 b_k - a_k b_k^2},\\ b_{k+1} &= b_k + \frac{3a_k^2(2a_k - b_k)(a_k + b_k)}{b_k^3 - 4a_k^2 b_k - a_k b_k^2}, \end{aligned} \quad (10)$$

with the initial conditions $a_0 = z/3$ and $b_0 = 1$. For $z \to 1$, the relevant fixed point (describing the infinite system, $k \to \infty$) is $a_\infty, b_\infty \to 0$; the width of the domains grows as $L_k \sim 4^k$ which is faster than the reach of the diffusive transport between them, as represented by a_k. With the scaling ansatz $a_k = 3^{-k}\alpha_k$ and $b_k = 3^{-k}\beta_k$, we resolve this boundary layer to find the fixed point $\beta_\infty = 3\alpha_\infty$ with the Jacobian eigenvalue $\lambda = 21$ that relates to the rescaling of time, $T_{k+1} = \lambda T_k$, via the Tauberian theorems [10,11,24]. Then, $L_{k+1} = 4L_k$ and $T_k \sim L_k^{d_w}$ from Eq. (1) finally yield $d_w^{RW} = \log_4(21)$.

For the quantum walk, the hopping operators now are matrices in coin space, and the algebra gets more involved. Iterating the matrix-valued RG flow in Eq. (9) numerically suggests that all matrices can be parametrized with merely two scalars, most conveniently in the form $\{A,B,C\} = \frac{a+b}{2}(P_{\{1,2,3\}} \cdot \mathcal{C}_G)$ and $M = \frac{a-b}{2}(\mathbb{I} \cdot \mathcal{C}_G)$, where the 3×3 matrices $[P_\nu]_{i,j} = \delta_{i,\nu}\delta_{\nu,j}$ (with $\sum_{\nu=1}^3 P_\nu = \mathbb{I}$) facilitate the shift of the νth component to a neighboring site. The RG flow closes for

$$\begin{aligned} a_{k+1} &= \frac{-9a_k + 5a_k^3 + 9b_k + 3a_k b_k - 17a_k^2 b_k - 3a_k^3 b_k + 3b_k^2 + 14a_k b_k^2 - 3a_k^2 b_k^2 - 18a_k^3 b_k^2}{-18 - 3a_k + 14a_k^2 + 3a_k^3 - 3b_k - 17a_k b_k + 3a_k^2 b_k + 9a_k^3 b_k + 5b_k^2 - 9a_k^2 b_k^2},\\ b_{k+1} &= \frac{-3a_k - a_k^2 + 3b_k + 4a_k b_k - 3a_k^2 b_k - b_k^2 + 3a_k b_k^2 + 6a_k^2 b_k^2}{6 + 3a_k - a_k^2 - 3b_k + 4a_k b_k + 3a_k^2 b_k - b_k^2 - 3a_k b_k^2}, \end{aligned} \quad (11)$$

with $a_0 = b_0 = z$. It can be shown that $|a_k| = |b_k| \equiv 1$ for all k, reducing the RG parameters to just two real phases for a_k, b_k.

As explained in Ref. [28], the classical fixed-point analysis above fails for the quantum walk. Unitarity demands that information about $\rho(\vec{x},t)$ has to be recovered from an integral involving $\tilde{\psi}_{\vec{x}}[a_k(z), b_k(z)]$ around the unit circle in the complex-z plane. It is the *scaling collapse* of $\{a,b\}_k(z) \sim f_{\{a,b\}}(\lambda^k \arg z)$, and, consequently, of any observable function of $\tilde{\psi}_{\vec{x}}$, over a finite support that allows us to approximate d_w recursively with arbitrary accuracy. An illustration of the collapse for, say, the phase of b_k is shown in Fig. 2. Equivalent plots can be found in the Appendix for MK4, HN3, and DSG.

To justify these RG predictions for d_w, we resort to direct simulation of quantum walks to test Eq. (1). Those simulations

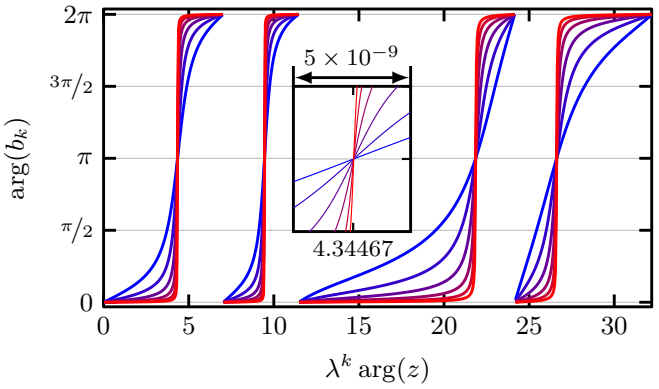

FIG. 2. (Color online) Scaling collapse for MK3 of the phase of b_k in Eq. (11) near the fixed point $z = 1$ with $\lambda = \sqrt{21}$. The inset shows the region around the first intersection. In the main panel, $k = 4,6,\ldots,14$, while $k = 50,52,\ldots 60$ for the inset, corresponding to a system size of MK3 with up to $N \approx 7^{60} \approx 10^{51}$ sites.

cannot reach as extreme a system size as RG, but the collapse of the probability density $\rho(x,t)$ over the entire network illustrates the consistency with the RG predictions, as shown in Fig. 3 for all four networks considered here.

IV. CONCLUSIONS

We have shown how to apply RG to obtain the scaling for the limit distribution in Eq. (1) for discrete-time quantum walks on several network for which RG is exact. This study demonstrates that RG can deliver unprecedented insights into the dynamics of quantum processes on systems that lack those symmetries familiar from lattices, hypercubes, trees, etc., such as translational invariance. While RG is limited to specific networks such as those considered here (which may not themselves be of technical importance), conceptually, the accumulation of the obtained results suggests a larger picture. Our findings hint at a deep, residual connection between classical and quantum walks based on the geometry of the network they share, which is surprising in light of the often dramatic quantum interference effects that distinguish quantum walks from random walks. The conjecture in Eq. (2) is likely not a trivial result. We have evidence that this simple relation holds only for the Grover coin, which has the property of being reflective, making it its own inverse. Other coins without that property, indeed, lead to different asymptotic limits, as we will describe elsewhere. This raises interesting questions regarding the range of possible *universality classes* of these results and their origin, a central concern of RG [37] that has remained largely unexplored for quantum walks [28]. In turn, it is straightforward to show that, asymptotically, random walks on these networks are independent of the specific choices for a Bernoulli coin. However, for quantum walks, the most general unitary coin matrix C for $r = 3$ would already contain six free parameters that could impact the dynamics in unforeseen ways and could lead to significant means of control.

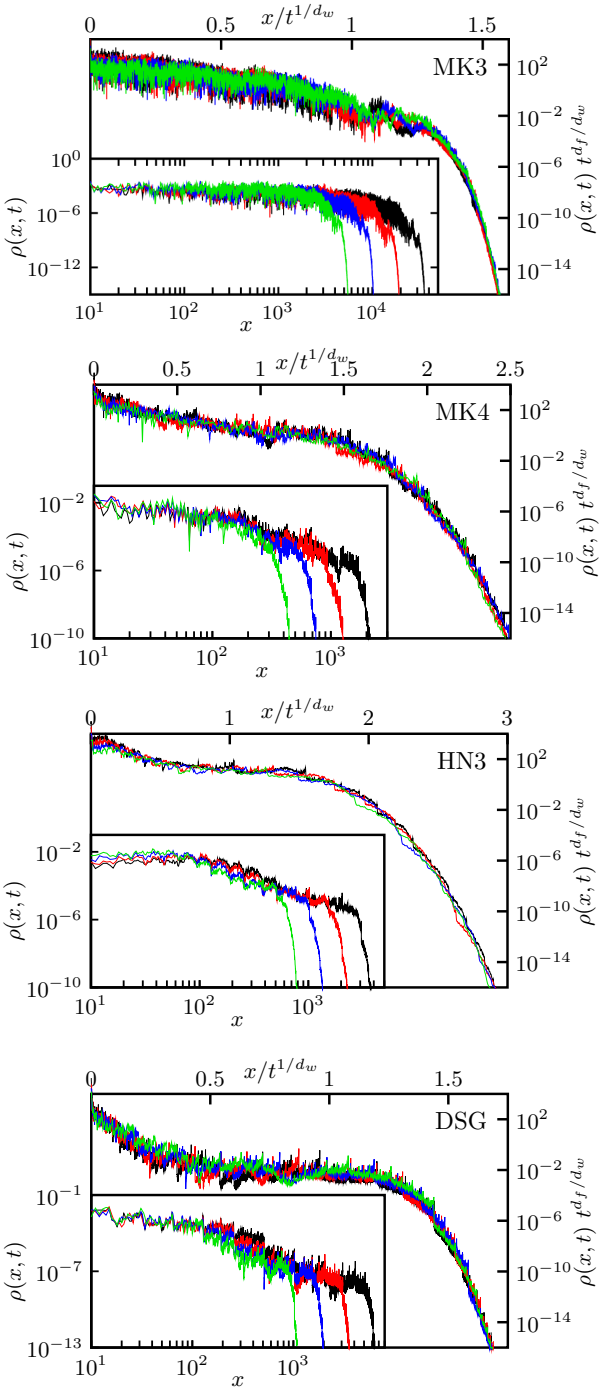

FIG. 3. (Color online) Data collapse of the probability density $\rho(|\vec{x}|,t)$ according to Eq. (1) with d_f and d_w given in Table I. The data are obtained by direct simulations of quantum walks on the four different networks in this study. The inset of each panel shows the raw data, from left to right for increasing time in each case. The first panel concerns MK3 with $N = 2 \times 7^8 \approx 10^7$ sites at times $t = 2^j$, $j = 13,\ldots,16$. In the main panel, the data are collapsed with $d_f = \log_4(7)$ and $d_w^{QW} = \log_4(21)/2$. The second panel concerns MK4 with $N = 2 \times 13^6 \approx 10^7$ sites at $t = 2^j$, $j = 12,\ldots,15$, collapsed with $d_f = \log_4(13)$ and $d_w^{QW} = \log_{16}(247/7)$. The third panel concerns HN3 with $N = 2^{24} \approx 1.7 \times 10^7$ sites at $t = 2^j$, $j = 11,\ldots,14$, collapsed with $d_f = 2$ and $d_w^{QW} = \log_4(24 - 8\sqrt{5})$. The fourth panel concerns DSG with $N = 3^{15} \approx 1.4 \times 10^7$ sites at $t = 2^j$, $j = 11,\ldots,14$, collapsed with $d_f = \log_2(3)$ and $d_w^{QW} = \log_2(5)/2$.

ACKNOWLEDGMENTS

S.B. and S.F. acknowledge financial support from the National Science Foundation (USA) through Grant No. DMR-1207431. S.B. acknowledges financial support from CNPq (Conselho Nacional de Desenvolvimento Científico e Tecnológico, Brasil) through Grant No. 400216/2014-0 in the "Ciência sem Fronteiras" program and thanks LNCC for its hospitality. R.P. acknowledges financial support from Faperj (Fundação Carlos Chagas Filho de Amparo à Pesquisa do Estado do Rio de Janeiro, Brasil) through Grant No. E-26/102.350/2013 and CNPq through Grants No. 304709/2011-5 and No. 474143/2013-9.

APPENDIX

While the methods presented for MK3 in the main text directly transfer to the other networks, we shall outline the procedure for them in more detail here. First, we consider the case of MK4, then we will discuss HN3 and DSG, which has been discussed previously [28]. MK4 is similar to MK3 except that it features a different degree for each site and thus establishes the conjecture for a different (rank $r = 4$) Grover coin than for the other networks considered here, which all use a Grover coin of rank $r = 3$. We have focused on the lowest-rank coins because higher-ranked coins generally make the algebra more complex. However, this $r = 4$ result demonstrates that the conjecture is likely robust, irrespective of the degree of sites.

RG for MK4. MK4 follows the same idea as MK3 as every edge is replaced by multiple nodes and edges from one generation to the next. The smallest four-regular graph that can be consistently labeled with four different edge types such that every node is connected to one of each kind contains six nodes (see Figs. 4). From the graphical representation, we can directly read off the linear system for the Laplace-transformed amplitudes on the interior nodes:

$$\begin{pmatrix}\tilde\psi_3\\ \tilde\psi_4\\ \tilde\psi_5\\ \tilde\psi_6\\ \tilde\psi_7\\ \tilde\psi_8\end{pmatrix} = \begin{bmatrix} A & 0 & M & B & 0 & 0 & D & C\\ 0 & 0 & B & M & D & C & 0 & A\\ 0 & A & 0 & D & M & B & C & 0\\ 0 & 0 & 0 & C & B & M & A & D\\ 0 & 0 & D & 0 & C & A & M & B\\ 0 & 0 & C & A & 0 & D & B & M \end{bmatrix} \begin{pmatrix}\tilde\psi_1\\ \tilde\psi_2\\ \tilde\psi_3\\ \tilde\psi_4\\ \tilde\psi_5\\ \tilde\psi_6\\ \tilde\psi_7\\ \tilde\psi_8\end{pmatrix}. \tag{A1}$$

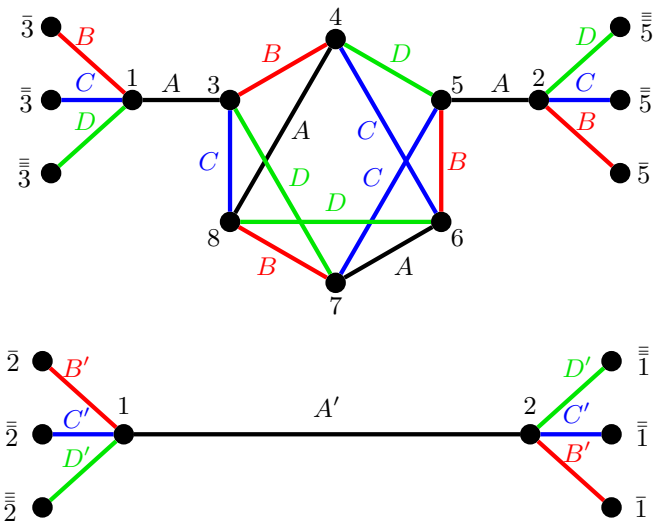

FIG. 4. (Color online) Iteration scheme for MK4. The six interior nodes $3,\ldots,8$ and all their connections (top) are replaced by direct connection between nodes 1 and 2 (bottom). The renormalized hopping parameter A' depends on all hopping matrices in the previous step. The construction of the network can be seen as the reverse process, inserting six nodes into every edge leaving the hopping parameter unchanged. The nodes labeled with overbars represent analogous nodes where the same rule is applied. The scheme for B, C, and D is obtained by cyclic permutation of the shown graphlets.

Once the solution in terms of $\tilde\psi_1$ and $\tilde\psi_2$ is found, we can plug it into the equations for, say, $\tilde\psi_1$,

$$\tilde\psi_1 = A\tilde\psi_3 + B\tilde\psi_{\bar3} + C\tilde\psi_{\bar{\bar3}} + D\tilde\psi_{\bar{\bar{3}}}, \tag{A2}$$

to find the renormalized system

$$\tilde\psi_1 = A'\tilde\psi_2 + B'\tilde\psi_{\bar2} + C'\tilde\psi_{\bar{\bar2}} + D'\tilde\psi_{\bar{\bar{2}}}. \tag{A3}$$

By studying the first few iterations, we choose the ansatz

$$\begin{aligned} A_k &= \frac{a+b}{2}(P_1\cdot\mathcal{C}_G), \quad B_k = \frac{a+b}{2}(P_2\cdot\mathcal{C}_G),\\ C_k &= \frac{a+b}{2}(P_3\cdot\mathcal{C}_G), \quad D_k = \frac{a+b}{2}(P_4\cdot\mathcal{C}_G),\\ M_k &= \frac{a-b}{2}\cdot(\mathbb{I}\cdot\mathcal{C}_G), \end{aligned} \tag{A4}$$

capturing the evolution of all matrices. P_ν are the 4×4 equivalents of the previously defined matrices [see Eqs. (A4)].

Here the recursions for the parameters read

$$a_{k+1} = \frac{-8a_k+5a_k^3+a_k^4+(8+4a_k-22a_k^2-a_k^3+5a_k^4)b_k+(4+21a_k+3a_k^2-30a_k^3-4a_k^4)b_k^2+a_k(5+13a_k-4a_k^2-16a_k^3)b_k^3}{-16-4a_k+13a_k^2+5a_k^3+(-4-30a_k+3a_k^2+21a_k^3+4a_k^4)b_k+(5-a_k-22a_k^2+4a_k^3+8a_k^4)b_k^2+(1+5a_k-8a_k^3)b_k^3},$$

$$b_{k+1} = \frac{-8b_k+b_k^3+a_k^3b_k(5+4b_k-16b_k^2)+a_k^2(4+13b_k-26b_k^2-12b_k^3)+a_k(8-12b_k-18b_k^2+b_k^3)}{-16-12a_k+a_k^2+a_k^3+2(2-13a_k-9a_k^2)b_k+(5+13a_k-12a_k^2-8a_k^3)b_k^2+4a_k(1+2a_k)b_k^3}, \tag{A5}$$

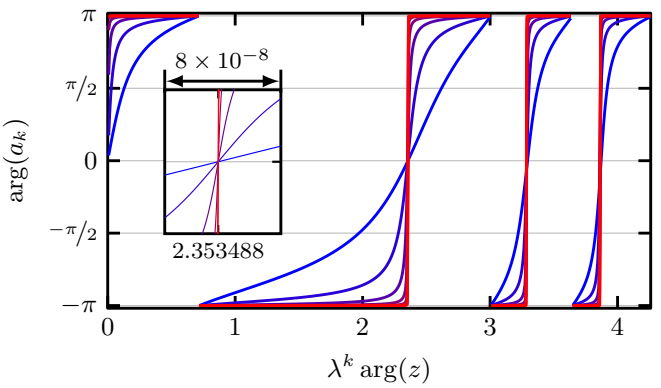

FIG. 5. (Color online) Rescaling for MK4 of the phase of the first RG parameter a_k in Eq. (A5) around the fixed point $z = 1$ with $\lambda = \sqrt{\frac{247}{7}}$. The insets show a magnification to illustrate the conversion towards a step function. In the main panel, $k = 2,6,...,14$ while $k = 20,22,...30$ for the inset. This corresponds to a system size of $N = 13^{30} \approx 10^{34}$.

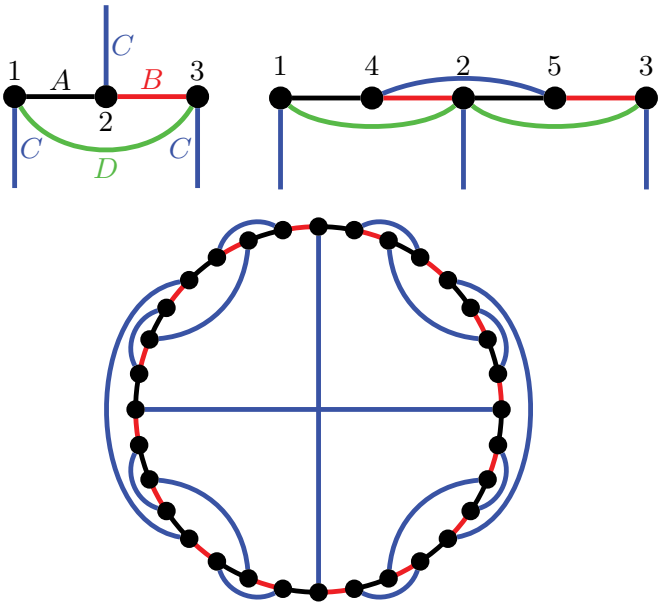

FIG. 6. (Color online) Illustration of the decimation scheme for HN3. Growing the network means inserting new nodes (4 and 5) and connecting them accordingly (top row). The graph at generation $k = 5$ is shown in the lower panel. The RG decimation requires an extra set of hopping matrices [D, orange (light gray)] in order to close the recursions, but these are not present in the actual network.

with $a_0 = b_0 = z$ as the initial conditions. These recursions resemble those in Eqs. (11), but the degrees of the polynomials in numerator and denominator are higher. This is a direct consequence of the higher number of sites eliminated during one iteration. Again, we have chosen a parametrization where $|a_{k+1}| = |b_{k+1}| = 1$ if $|a_k| = |b_k| = 1$. The rescaling of the phase of a_k is shown in Fig. 5. The direct simulation for MK4 in Fig. 3 again confirms the RG prediction.

RG for HN3. The derivation of RG equations for HN3 (see Fig. 6) is slightly more complicated than the above calculations for MK3 and MK4 for three reasons. First, the recursion on HN3 requires the introduction of a fourth hopping parameter D, which is not present in the actual graph but becomes necessary to close the RG flow. Second, the symmetry of the hoppings is not preserved by the recursions. This means, after one decimation step, the matrix representing the hop from site 1 to site 2 is no longer identical to the one from site 2 to site 1. Third, the rules leading to HN3 inherently distinguish between even and odd sites. As a result, the self-interaction terms become different for those two groups. If we make the ansatz

$$A = \begin{bmatrix} \frac{b-a}{4} & \frac{a+b+2c}{4} & 0 \\ 0 & 0 & 0 \\ 0 & 0 & 0 \end{bmatrix} \cdot \mathcal{C}_G \quad C = \begin{bmatrix} 0 & 0 & 0 \\ 0 & 0 & 0 \\ 0 & 0 & z \end{bmatrix} \cdot \mathcal{C}_G$$

$$B = \begin{bmatrix} 0 & 0 & 0 \\ \frac{a+b+2c}{4} & \frac{b-a}{4} & 0 \\ 0 & 0 & 0 \end{bmatrix} \cdot \mathcal{C}_G \quad D = \begin{bmatrix} 0 & \frac{b-a}{4} & 0 \\ 0 & 0 & 0 \\ 0 & 0 & 0 \end{bmatrix} \cdot \mathcal{C}_G$$

$$M_1 = \begin{bmatrix} \frac{a+b-2c}{4} & \frac{b-a}{4} & 0 \\ \frac{b-a}{4} & \frac{a+b-2c}{4} & 0 \\ 0 & 0 & 0 \end{bmatrix} \cdot \mathcal{C}_G$$

$$M_2 = \begin{bmatrix} \frac{a+b-2c}{4} & 0 & 0 \\ 0 & \frac{a+b-2c}{4} & 0 \\ 0 & 0 & 0 \end{bmatrix} \cdot \mathcal{C}_G, \tag{A6}$$

we can take everything into account by writing the linear system corresponding to the top right graphlet in Fig. 6:

$$\begin{aligned} \tilde{\psi}_4 &= A^T \tilde{\psi}_1 + B^T \tilde{\psi}_2 + M_1 \tilde{\psi}_4 + C \tilde{\psi}_5, \\ \tilde{\psi}_5 &= A^T \tilde{\psi}_2 + B^T \tilde{\psi}_3 + C^T \tilde{\psi}_4 + M_1 \tilde{\psi}_5. \end{aligned} \tag{A7}$$

Here A^T represents the transpose of A. As it turns out, this correctly describes the hopping in different directions (left or right in the figure).

By solving these equations for $\tilde{\psi}_4$ and $\tilde{\psi}_5$ and inserting the result into the equations for the remaining sites,

$$\begin{aligned} \tilde{\psi}_1 &= M_2 \tilde{\psi}_1 + D \tilde{\psi}_2 + D^T \tilde{\psi}_2' + A \tilde{\psi}_4 + B^T \tilde{\psi}_5' + C \tilde{\psi}_*, \\ \tilde{\psi}_2 &= D \tilde{\psi}_1 + M_2 \tilde{\psi}_2 + D^T \tilde{\psi}_3 + B^T \tilde{\psi}_4 + A \tilde{\psi}_5 + C \tilde{\psi}_*, \end{aligned} \tag{A8}$$

where we omitted the equation for $\tilde{\psi}_3$ because it is identical to the first one. Every node is connected to a node of unknown index $\tilde{\psi}_*$, but the corresponding hopping matrix C does not change. After some algebra, we find the following recursion equations for the three RG variables:

$$\begin{aligned} a_{k+1} &= \frac{c_k(-3+z) - b_k[-3+z+c_k(-2+6z)]}{6 - b_k + c_k + (-2+3b_k-3c_k)z}, \\ b_{k+1} &= \frac{c_k(3+z) - b_k[3+z+c_k(2+6z)]}{-6 + b_k - c_k + (-2+3b_k-3c_k)z}, \\ c_{k+1} &= \frac{c_k + a_k(-1+2c_k)}{2 + a_k - c_k}, \end{aligned} \tag{A9}$$

with the initial conditions

$$a_0 = \frac{z^2(1-3z)}{3-z}, \quad b_0 = \frac{z^2(1+3z)}{3+z}, \quad c_0 = z^2. \tag{A10}$$

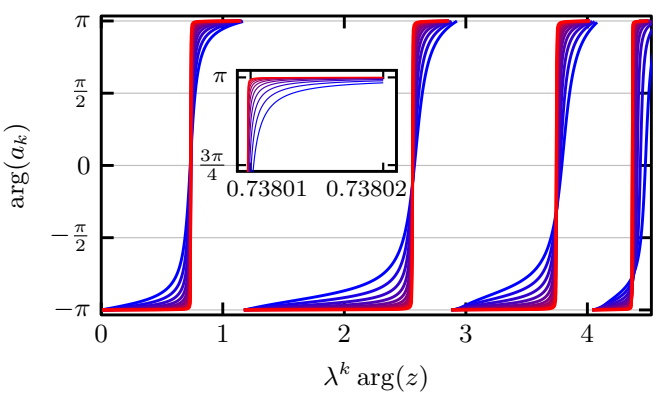

FIG. 7. (Color online) Rescaling for HN3 of the phase of the first RG parameter a_k in Eq. (A9) around the fixed point $z = 1$. The inset shows a magnification to illustrate the conversion towards a step function. In the main panel, $k = 10,12,\ldots,30$, while $k = 60,62,\ldots 80$ for the inset. This means the largest system size is $N \approx 10^{24}$. Here $\lambda = 2^{1-\log_2(\varphi)/2}$, where $\varphi = (\sqrt{5}+1)/2$ is the "golden section" [42].

Again, we have chosen our ansatz such that the variables remain modulus 1 when they start out that way. This time we show the rescaling of the argument of the first RG parameter in Fig. 7. As verification, we have also scaled the numerically obtained probability density function in Fig. 3.

RG for DSG. Finally, we consider the DSG again [28] with this approach (see Fig. 8). In order to make it renormalizable, we have to introduce a directionality represented by the arrows for A and B. This just means that applying one hopping matrix, say A, twice describes the hopping from site 1 to 2 (over site 3), and not site 1 to 3 back to 1. The matrix C is not affected by this.

The linear system we need to solve in this case reads

$$\begin{pmatrix}\tilde\psi_4\\ \tilde\psi_5\\ \tilde\psi_6\\ \tilde\psi_7\\ \tilde\psi_8\\ \tilde\psi_9\end{pmatrix} = \begin{bmatrix} B & 0 & 0 & M & A & 0 & 0 & 0 & C\\ A & 0 & 0 & B & M & C & 0 & 0 & 0\\ 0 & B & 0 & 0 & C & M & A & 0 & C\\ 0 & A & 0 & 0 & 0 & B & M & C & 0\\ 0 & 0 & B & 0 & 0 & 0 & C & M & A\\ 0 & 0 & A & C & 0 & 0 & 0 & B & M \end{bmatrix} \begin{pmatrix}\tilde\psi_1\\ \tilde\psi_2\\ \tilde\psi_3\\ \tilde\psi_4\\ \tilde\psi_5\\ \tilde\psi_6\\ \tilde\psi_7\\ \tilde\psi_8\\ \tilde\psi_9\end{pmatrix}. \quad \text{(A11)}$$

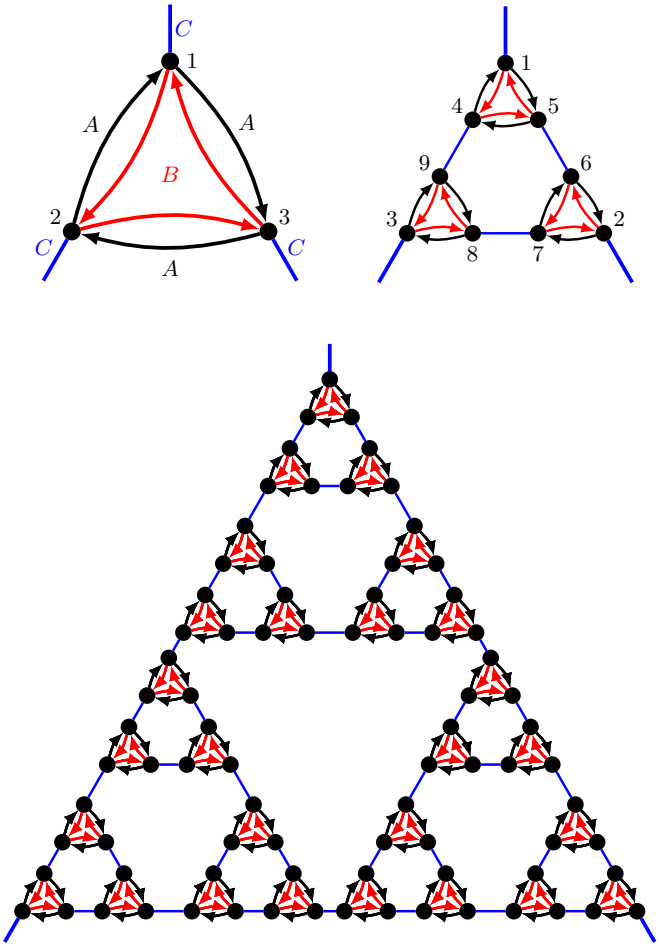

FIG. 8. (Color online) The well-known recursion generating the DSG (top row). To make the positions of the hopping matrices also self-similar, we have to introduce directionality of the hopping matrices A and B. The third one, C, is still symmetric. The lower panel shows the system at generation 4.

The results then have to be plugged into the equations for $\tilde\psi_1,\ldots,\tilde\psi_3$:

$$\begin{aligned}\tilde\psi_1 &= A\tilde\psi_4 + B\tilde\psi_5 + C\tilde\psi'_{2,3},\\ \tilde\psi_2 &= A\tilde\psi_6 + B\tilde\psi_7 + C\tilde\psi''_1,\\ \tilde\psi_1 &= A\tilde\psi_8 + B\tilde\psi_9 + C\tilde\psi'''_1.\end{aligned} \quad \text{(A12)}$$

Here the algebra is very involved, and we have shown elsewhere [28] how it can done. There, we showed the scaling of the parameters and deduced d_w^{QW} from it using the RG. The scaling plot obtained by direct simulations in Fig. 3 confirms again the conjecture.

[1] H. B. Perets, Y. Lahini, F. Pozzi, M. Sorel, R. Morandotti, and Y. Silberberg, Phys. Rev. Lett. **100**, 170506 (2008).

[2] C. Weitenberg, M. Endres, J. F. Sherson, M. Cheneau, P. Schauss, T. Fukuhara, I. Bloch, and S. Kuhr, Nature (London) **471**, 319 (2011).

[3] L. Sansoni, F. Sciarrino, G. Vallone, P. Mataloni, A. Crespi, R. Ramponi, and R. Osellame, Phys. Rev. Lett. **108**, 010502 (2012).

[4] A. Crespi, R. Osellame, R. Ramponi, V. Giovannetti, R. Fazio, L. Sansoni, F. D. Nicola, F. Sciarrino, and P. Mataloni, Nat. Photonics **7**, 322 (2013).

[5] A. M. Childs, Phys. Rev. Lett. **102**, 180501 (2009).
[6] A. M. Childs, D. Gosset, and S. Webb, Science **339**, 791 (2013).
[7] L. K. Grover, Phys. Rev. Lett. **79**, 325 (1997).
[8] *Random Walks and Their Applications in the Physical and Biological Sciences*, edited by M. F. Shlesinger and B. J. West (AIP, New York, 1984).
[9] S. Havlin and D. Ben-Avraham, Adv. Phys. **36**, 695 (1987).
[10] G. H. Weiss, *Aspects and Applications of the Random Walk* (North-Holland, Amsterdam, 1994).
[11] B. D. Hughes, *Random Walks and Random Environments* (Oxford University Press, Oxford, 1996).
[12] D. Aharonov, A. Ambainis, J. Kempe, and U. Vazirani, in *Proceedings of 33rd Annual ACM Symposium on Theory of Computing (STOC 2001)* (ACM, New York, 2001), pp. 50–59.
[13] A. Ambainis, E. Bach, A. Nayak, A. Vishwanath, and J. Watrous, in *Proceedings of the Thirty-Third Annual ACM Symposium on Theory of Computing, STOC '01* (ACM, New York, 2001), pp. 37–49.
[14] E. Bach, S. Coppersmith, M. P. Goldschen, R. Joynt, and J. Watrous, J. Comput. Syst. Sci. **69**, 562 (2004).
[15] A. M. Childs, E. Farhi, and S. Gutmann, Quantum Inf. Process. **1**, 35 (2002).
[16] A. M. Childs and J. Goldstone, Phys. Rev. A **70**, 022314 (2004).
[17] N. Konno, in *Quantum Potential Theory*, edited by U. Franz and M. Schürmann, Lecture Notes in Mathematics Vol. 1954 (Springer, Heidelberg, 2008), pp. 309–452.
[18] F. Magniez, A. Nayak, P. C. Richter, and M. Santha, in *Proceedings of the Twentieth Annual ACM-SIAM Symposium on Discrete Algorithms, SODA '09* (Society for Industrial and Applied Mathematics, Philadelphia, 2009), pp. 86–95.
[19] Y. Shikano and H. Katsura, Phys. Rev. E **82**, 031122 (2010).
[20] E. Venegas-Andraca, Quantum Inf. Process. **11**, 1015 (2012).
[21] R. Portugal, *Quantum Walks and Search Algorithms* (Springer, Berlin, 2013).
[22] W. Feller, *An Introduction to Probability Theory and Its Applications* (Wiley, New York, 1966), Vol. 1.
[23] J.-P. Bouchaud and A. Georges, Phys. Rep. **195**, 127 (1990).
[24] S. Redner, *A Guide to First-Passage Processes* (Cambridge University Press, Cambridge, 2001).
[25] G. Grimmett, S. Janson, and P. F. Scudo, Phys. Rev. E **69**, 026119 (2004).
[26] N. Konno, Quant. Info. Proc. **1**, 345 (2002).
[27] E. Segawa and N. Konno, Int. J. Quantum Inf. **6**, 1231 (2008).
[28] S. Boettcher, S. Falkner, and R. Portugal, Phys. Rev. A **90**, 032324 (2014).
[29] N. Konno, J. Math. Soc. Jpn. **57**, 1179 (2005).
[30] A. Ambainis, SIAM J. Comput. **37**, 210 (2007).
[31] A. M. Childs, R. Cleve, E. Deotto, E. Farhi, S. Gutmann, and D. A. Spielman, in *Proceedings of the Thirty-Fifth Annual ACM Symposium on Theory of Computing, STOC '03* (ACM, New York, 2003), pp. 59–68.
[32] A. Blumen and O. Mülken, Phys. Rep. **502**, 37 (2011).
[33] G. D. Paparo, M. Müller, F. Comellas, and M. A. Martin-Delgado, Sci. Rep. **3**, 2773 (2013).
[34] D. A. Meyer, J. Stat. Phys. **85**, 551 (1996).
[35] R. Portugal, S. Boettcher, and S. Falkner, Phys. Rev. A **91**, 052319 (2015).
[36] A. N. Berker and S. Ostlund, J. Phys. C **12**, 4961 (1979).
[37] M. Plischke and B. Bergersen, *Equilibrium Statistical Physics*, 2nd ed. (World Scientific, Singapore, 1994).
[38] S. Boettcher and B. Gonçalves, Europhys. Lett. **84**, 30002 (2008).
[39] V. Singh and S. Boettcher, Phys. Rev. E **90**, 012117 (2014).
[40] S. Boettcher, S. Falkner, and R. Portugal, J. Phys. Conf. Ser. **473**, 012018 (2013).
[41] E. Domany, S. Alexander, D. Bensimon, and L. P. Kadanoff, Phys. Rev. B **28**, 3110 (1983).
[42] M. Livio, *The Golden Ratio: The Story of Phi, the World's Most Astonishing Number* (Broadway Books, New York, 2003).